Journal of the Civil Engineering Forum, January 2026, 12(1):89-103
DOI 10.22146/jcef.24124
Available Online at https://jurnal.ugm.ac.id/v3/jcef/issue/archive

Hydrated Lime–Based Coating for Cool Pavement Technologies: Evaluation of Durability and Thermal Performance

Muhammad Khuzamy[1], Taqia Rahman[1*], Imtiaz Ahmed[2], Syed Bilal Ahmed Zaidi[3]
[1]Department of Civil and Environmental Engineering, Universitas Gadjah Mada, Yogyakarta, INDONESIA
[2]AtkinsRéalis, Nottingham, UNITED KINGDOM
[3]Taxila Institute of Transportation Engineering, University of Engineering and Technology, Taxila, PAKISTAN
*Corresponding author: taqia.rahman@ugm.ac.id

SUBMITTED 26 August 2025 **REVISED** 20 October 2025 **ACCEPTED** 25 October 2025

ABSTRACT Heat-reflective pavement coatings are commonly employed for road cooling and to mitigate Urban Heat Island (UHI) effects by reflecting solar radiation and reducing surface temperatures. However, their cooling efficiency diminishes over time due to abrasion, soiling, UV exposure, and environmental aging, which degrade the reflective polymer layer. As a cost-effective alternative, hot-rolled hydrated lime (HL) applied to pavement surfaces has emerged, forming a light-coloured mineral layer that enhances reflectivity and potentially reduces pavement temperature. This study investigates hydrated lime (HL) as a mineral-based alternative, applied through hot-rolling to form a reflective surface layer that is compatible with conventional asphalt practices. Its performance was evaluated through laboratory thermal simulations (day–night cycling) and abrasion wear testing and compared with three commercial paint-based HRCs: epoxy resin–TiO_2 and acrylic emulsion–TiO_2. The results show that HL coatings achieved surface temperature reductions of up to 21.89 °C compared to uncoated asphalt, exceeding the best-performing paint-based sample (White-AE, 19.29 °C), suggesting that HL has strong potential as an effective reflective coating. This was achieved with a formulation of fine HL particles (No. 400 mesh) at a higher dosage (200 g/m^2). In abrasion resistance tests, HL outperformed paint-based HRCs, with lower mass losses (0.6–1.3 g vs. 0.8–1.5 g), which was attributed to stronger adhesion and particle embedment. In addition, post-abrasion tests revealed that HL samples retained better thermal stability, with smaller temperature increases (ΔT: 5.9–6.8 °C) than HRCs (ΔT: 6.3–7.2 °C). Based on these outcomes, HL applied at 200 g/m^2 using fine particles (No.400 mesh) is recommended as the optimal formulation for maximizing cooling performance and surface durability. Overall, these findings suggest that hot-rolled HL is a durable, low-cost, and effective alternative cooling strategy to popular HRCs for UHI mitigation.

KEYWORDS Cool pavements; Hydrated lime; UHI mitigation; Heat reflective coating; Road cooling; Asphalt.

1 INTRODUCTION

Rapid urbanization has accelerated global land use change and urban spatial expansion (Güneralp et al., 2020; Rahman et al., 2025a). Projections indicate that by 2050, global urban land area will increase by approximately 78–171%, with Asia and Africa collectively contributing to nearly two-thirds of this growth—46–49% and 16–25%, respectively (Huang et al., 2019). In Europe, urban areas are expected to expand by 7% by 2030 (Güneralp et al., 2020). Such expansion intensifies the Urban Heat Island (UHI) effect, in which urban areas exhibit higher surface and air temperatures than their rural surroundings (Ibrahim et al., 2018). On average, the UHI effect elevates daily summer temperatures by 0.5–0.7 °C, and in densely developed urban cores, the increase can reach up to 3 °C (Huang et al., 2019).

In addition to human-induced urbanization, the intensity of the UHI effect is further influenced by environmental and spatial factors such as vegetation cover (44%), seasonality (33%) and diurnal variation (25%) (Deilami et al., 2018). Among these, the decline in urban vegetation—driven by massive infrastructure development—has significantly contributed to elevated surface temperatures. The conversion of vegetated areas into impervious built-up zones such as residential complexes, commercial areas, and extensive road networks has altered the thermal balance of urban landscapes (Fathan et al., 2025; Mathan and Krishnaveni, 2019).

One of the most critical contributors to this thermal imbalance is pavement infrastructure, which occupies approximately 30–40% of the total urban surface area (Cheela et al., 2021; Liu et al., 2018). Of this, an estimated 75–80% comprises dark-coloured pavements, particularly asphalt, which exhibit low albedo values and high thermal absorption (Cheela et al., 2021; Huang et al., 2020). For instance, conventional asphalt pavement typically has an albedo of approximately 0.05–0.10, meaning it reflects only 5–10% of in-

coming solar radiation while absorbing 90–95% (Rahman et al., 2025*a*). This high absorptivity leads to substantial heat accumulation and gradual release, resulting in surface temperatures that can reach up to 59.4 °C under peak conditions (Boujelbene et al., 2023). This persistent heat retention not only intensifies the UHI effect but also contributes to premature pavement deterioration (Nugroho et al., 2025), increased cooling energy demand, and elevated thermal discomfort in urban environments (Rajagopal et al., 2023).

The impacts of the UHI phenomenon extend far beyond elevated temperatures. They include increased energy consumption, deteriorating air quality, heightened health risks, and reduced environmental resilience (Vujovic et al., 2021). UHI-induced warming can increase building cooling energy demand by 10–120%, placing additional pressure on power generation systems (Huang et al., 2019). This increased energy demand often results in higher emissions of pollutants such as carbon monoxide (CO), carbon dioxide (CO_2), sulphur dioxide (SO_2), nitrogen oxides (NO_x), and particulate matter—compounds known to exacerbate respiratory and cardiovascular conditions, including bronchitis and airway irritation (Vujovic et al., 2021).

The chain of consequences associated with UHI underscores the urgent need for effective mitigation strategies. Among the most widely studied approaches are cool pavement technologies, which aim to lower surface temperatures by increasing reflectivity (Wong et al., 2024), enhancing evaporation (Ega Fajar et al., 2025; Rahman et al., 2025*b*), or modifying thermal properties (Shamsaei et al., 2024). One widely adopted cool pavement solution is the application of heat-reflective coatings (HRCs), which are designed to increase surface albedo and reduce solar heat gain (Rahman et al., 2023). These coatings form a thin, high-reflectivity layer on the pavement surface, enabling significant reductions in both surface and near-surface air temperatures by reflecting a larger portion of incoming solar radiation (Alhaqi et al., 2024; Wang et al., 2021). Field and simulation studies have shown that HRCs can reduce peak pavement surface temperatures by up to 30 °C compared to uncoated asphalt, and in some cases even achieve sub-ambient surface temperatures under certain conditions (Elmagri et al., 2024; Mandal et al., 2020).

However, these benefits are offset by several limitations. Rahman et al. (2024) reported that typical HRCs exhibit functional durability of only about one year, especially under moderate to heavy traffic loads. Additionally, HRCs often suffer from low abrasion resistance, high application costs, and concerns about the environmental impact of certain chemical constituents used in the coating formulation (Man et al., 2021). These limitations reduce their viability for long-term or large-scale implementation, particularly in high-wear roadway segments or cost-sensitive infrastructure projects.

A promising alternative to polymer-based paint HRC is the application of hydrated lime ($Ca(OH)_2$) directly to the pavement surface during or immediately after compaction, followed by hot pressing. This method forms a thin, light-coloured mineral layer that increases surface reflectivity, thereby reducing solar heat absorption and lowering surface temperatures. When properly applied, the reflective layer is expected to remain effective for up to five years under typical field conditions (Emery et al., 2014). In addition to its thermal benefits, hydrated lime (HL) is cost-effective, widely available, and compatible with standard paving practices (Emery et al., 2014; Mondal et al., 2023). A recent study by Man et al. (2021) further demonstrated that hot-pressed hydrated lime can lower asphalt surface temperatures by approximately 10 °C—slightly less than conventional paint-based coatings but at a substantially lower cost.

Based on the above background, hydrated lime (HL) offers a potentially more cost-effective and abrasion-resistant alternative to paint-based heat-reflective coatings (HRC) while providing comparable surface cooling benefits. However, no previous studies have comprehensively evaluated its thermal and mechanical performance under varying application parameters in direct comparison with HRC. To address this gap, the present study aims to assess the abrasion resistance and thermal performance of hot-pressed HL as a reflective surface treatment and compare it with conventional paint-based HRC. This was conducted through laboratory experiments involving surface temperature measurements and abrasion resistance tests, incorporating variations in paint formulations for HRC and different particle sizes and spreading dosages for HL. The information on hydrated lime (HL) as an alternative to paint-based HRC is important for assessing its impact on cooling performance, durability, and practical use in pavements.

2 RESEARCH OBJECTIVE AND APPROACH

The main objective of this study is to evaluate the thermal performance and abrasion resistance of paint-based heat-reflective coatings (HRCs) and hot-pressed hydrated lime (HL) as reflective treatments for asphalt pavements. HL was selected for its potential as a more durable, cost-effective alternative, while water-based acrylic and oil-based epoxy were used to represent commonly used polymer binders in HRCs. In addition, the study assesses the effect of surface abrasion on the retained thermal performance of these coatings after wear. The experimental setup is illustrated in Figure 1. For this purpose, asphalt slabs measuring 306 $\times$ 306 $\times$ 50 mm were compacted and subsequently cut

into four smaller specimens (15 × 15 × 5 cm). This specimen size is commonly used in laboratory thermal asphalt tests, as reported by previous studies (Anting et al., 2017; Pan et al., 2022). Three types of HRCs were applied to the asphalt surface: epoxy resin (white and blue variants), acrylic emulsion, and a commercial reflective paint (BeCool). For HL, two particle sizes (No. 200 – 75 µm and No. 400 – 38 µm) were tested across four spreading dosages (50, 100, 150, and 200 g/m^2) (Alhaqi et al., 2024; Emery et al., 2014; Man et al., 2021). Coatings were applied by dry spreading (HRCs) and hot pressing (HL) onto clean, uncontaminated slab surfaces at room temperature (25 °C).

To measure internal temperature responses under heating and cooling simulations, thermocouples were embedded 2.5 cm below the surface (Figure 1), with thermal grease used to ensure proper contact. Samples were then exposed to tungsten iodine lamps (2 × 500 W) inside an insulated heating box (75 cm height) to simulate maximum solar radiation (1000 W/m^2) and record surface temperature under controlled indoor conditions. These lamps were selected because their spectral distribution closely resembles natural sunlight in the infrared range, and their combined power output effectively replicates typical solar intensity, making them suitable for accelerated laboratory thermal testing (Zheng et al., 2020). To assess mechanical durability, all coated samples were tested for abrasion resistance using a wet track abrasion machine operated in a dry configuration. After abrasion testing, specimens were re-tested for thermal performance under the same heating conditions to determine the effect of surface wear. Results were analysed to understand how coating durability influences cooling effectiveness, with the aim of identifying practical strategies for enhancing the lifespan and performance of cool pavement technologies.

3 MATERIALS AND METHODS

3.1 Materials

3.1.1 Asphalt Binders

In this study, an unmodified asphalt binder with a 60/70 penetration grade was selected for preparing the asphalt mixtures. The binder's essential physical characteristics—including its kinematic viscosity at 135 °C, penetration at 25 °C, softening point, and ductility—are summarized in Table 1 (Nugroho et al., 2025). This binder was used to produce asphalt slabs that served as the substrate for the application of surface reflective treatments.

Table 1. Properties of asphalt pen 60/70 used in this research (Nugroho et al., 2025)

Binder Properties	Result
Mass loss after TFOT (%)	0.011
Penetration at 25 °C (0.1 mm)	64
Ductility at 25 °C (cm)	>140
Kinematic viscosity at 135 °C (cSt)	410
Softening point (°C)	51
Flash point (°C)	319
Specific gravity	1.034
Solubility in Trichloroethylene (%)	99.7

3.1.2 Aggregate

The andesite aggregate used in this study for asphalt mixtures exhibited moderate abrasion resistance (20.2%), low fine particle content, strong bitumen adhesion (≥ 95%), and high angularity (47.4%), indicating good interlocking capacity. Key mechanical properties—including abrasion, surface texture, elongation, and soundness—are summarized in Table 2.

Table 2. Properties of aggregates used in this research

Aggregate Properties	Result
Abrasion	20.2%
Crushed particles in coarse aggregates	95/90
Flat and elongated aggregates	5%
Soundness	0.92%
Aggregate adhesiveness to bitumen	>95%
Sand equivalent	93.2%
Angularity	45.2%
Clay lumps and friable particles	0.03%

3.1.3 Asphalt Mixtures

This study utilized asphalt mixtures with the gradation illustrated in Figure 2, following the mixture gradation for asphalt concrete wearing course and aligned with Indonesian road construction standards (Kementerian PUPR, 2004). Sieve analysis was conducted using ASTM E11 specifications, with the maximum aggregate size of 19 mm (3/4 inch). To determine the optimal binder content, the Marshall mix design procedure was followed (ASTM, 2020*b*). The mixing process began by heating 1200 g of aggregate to 160 °C and bitumen to the same temperature before mixing. The mixture was

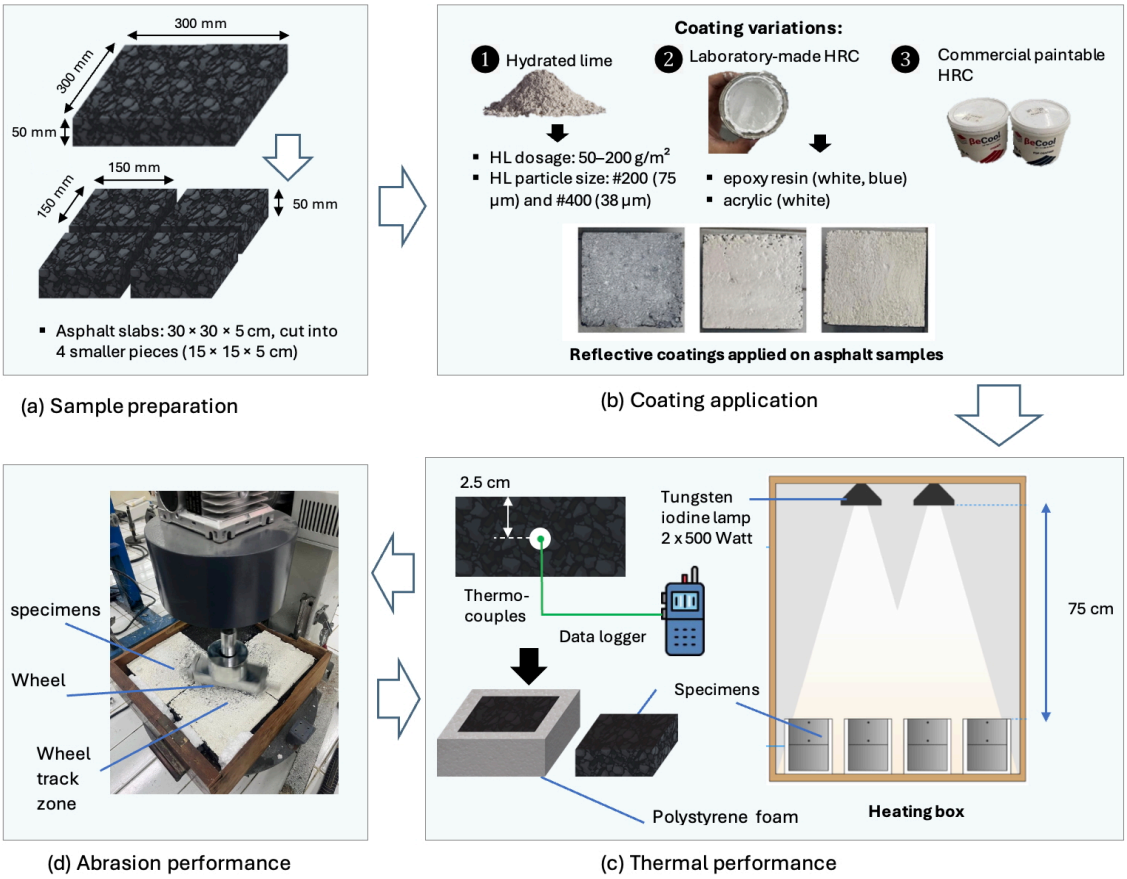

Figure 1 Experimental setup of the research.

homogenized and placed into a mold, then compacted at 140 °C using a Marshall hammer delivering 75 blows per face. The target air void content was set to 4 to 5%. From the test, the optimum asphalt binder content was determined to be 5.22%. At this content, the asphalt mixtures exhibited an average air void in total mix (VITM) of 4.81%.

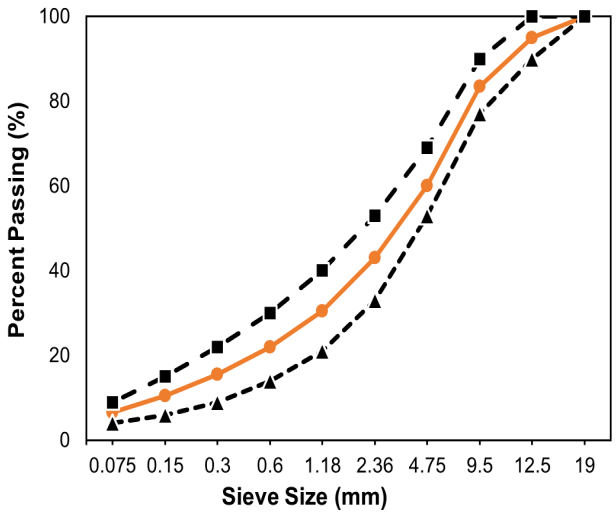

Figure 2 Aggregate gradation for asphalt mixture.

3.1.4 Hydrated Lime

Hydrated lime (HL), or calcium hydroxide ($Ca(OH)_2$), used in this study is an inorganic compound produced by slaking quicklime (CaO) with water. It is a white, strongly alkaline powder known for its chemical reactivity and ability to form strong bonds with asphalt binders. Its portlandite structure—characterized by its hexagonal symmetry and layered arrangement—underpins its high reflectivity, making it suitable for cooling applications (Iizuka et al., 2013). The HL used was in the form of fine, heterogeneous granules of varying sizes, applied in No. 200 (75 µm) and No. 400 (38 µm) mesh particle sizes to evaluate their effects on thermal performance and abrasion resistance. For each particle size, four application rates were used, 50, 100, 150, and 200 g/m² (Table 4). Due to its hygroscopic nature, HL readily absorbs moisture from the air, and its ultrafine particles tend to clump when exposed to ambient humidity (Abu-Halimeh, 2007). To address this, particle size separation was carried out in accordance with ASTM C110 (ASTM, 2020*a*). The procedure involved spreading HL evenly on an iron tray and drying it in an oven at 105 °C for 2–3 hours until a constant weight was reached. The dried material was then sieved using No.100, No.200, and No.400 mesh sieves on a mechanical sieve shaker for 30 minutes. After sieving, the

Table 3. Paint-based heat-reflective coating (HRC) samples and designations

Samples (Designation)[a]	Binder / Organic Polymers	Filler, TiO_2	Other additives[b]
White-ER	34.8%	30.4	34.8
White-AE	34.8%	30.4	34.8
White-BC	Proprietary (BeCool)	–	–

[a] ER = Epoxy Resin, AE = Acrylic Emulsion, BC = BeCool reflective paint.
[b] Additives include hardener/coalescing agents, dispersant, and defoamer.

separated particles were stored in sealed containers in a dry environment to prevent moisture uptake and agglomeration.

3.1.5 Paint-Based Heat reflective Coatings (HRC)

In this study, three paint-based heat-reflective coatings (HRCs) were evaluated: two laboratory-formulated coatings and a commercially available product. Pain-based HRCs incorporate a blend of organic binders and inorganic reflective materials to achieve solar reflectance (Rahman et al., 2024; Xie et al., 2015). In such formulations, organic polymers serve as the adhesive matrix, securing the components in place, while inorganic fillers enhance the surface's ability to reflect solar energy. In this study, two types of polymer bases were employed: water-based acrylic emulsion and oil-based epoxy resin, as they are commonly used binders in HRCs. Both types were combined with titanium dioxide (TiO_2), a well-known reflective white pigment, without the addition of color pigments. To refine the coating properties, various functional additives were incorporated. These include hardeners to promote epoxy curing, coalescing agents to ensure film formation, dispersants to stabilize the mixture, defoamers to eliminate entrapped air, and matting agents to reduce surface gloss. The detailed component breakdown for both coating types is presented in Table 3. Formulation ratios were adapted from prior studies by Li and Xie (2020); Xie et al. (2019) to ensure compatibility and effectiveness.

In addition to the laboratory-prepared coatings, a commercial paint, BeCool, was also used. It is a two-layer reflective coating system incorporating nano microspheres as the reflective component, with a solar reflectance of 0.77 and thermal emittance of 0.88. BeCool is commonly applied to roofs and is intended to reduce heat transfer in hot-humid climates.

3.1.6 Specimen Preparation

To create the specimen for testing, slab-shaped asphalt mixtures measuring 306 mm × 306 mm × 50 mm were fabricated using an asphalt mixing machine and a rut sample forming machine, in accordance with ASTM D8079–23 standards (ASTM, 2016). The preparation process began with drying the aggregates at 160 °C, followed by heating the asphalt binder to the required mixing temperature. Both components were then thoroughly blended at 145 °C using the asphalt mixer. The hot mixture was poured into a slab mold and compacted using a rut sample forming machine through 40 loading passes. After compaction, the mixture—along with the mould—was allowed to cool naturally to ambient temperature (approximately 25 °C). Once cooled, the compacted slab was removed from the mold and precisely cut using a stone cutter into four equal sections, each measuring approximately 150 mm × 150 mm × 50 mm with a 3 mm blade thickness (Figure 1(a)).

A total of 24 asphalt slab specimens (Figure 3) were prepared, including uncoated controls, three paint-based heat-reflective coatings (BeCool, epoxy, and acrylic), and eight hydrated lime (HL) surface treatments using

Table 4. Hydrated lime (HL) samples and designations

Particle Size	Surface application rate			
	50 g/m^2	100 g/m^2	150 g/m^2	200 g/m^2
No.200 (75 µm)	H2-50	H2-100	H2-150	H2-200
No.400 (38 µm)	H4-50	H4-100	H4-150	H4-200

Designation Rule: H = Hydrated Lime; 2 = Particle size No.200 (75 µm); 4 = Particle size No.400 (38 µm); last number = spreading dosage (g/m^2).

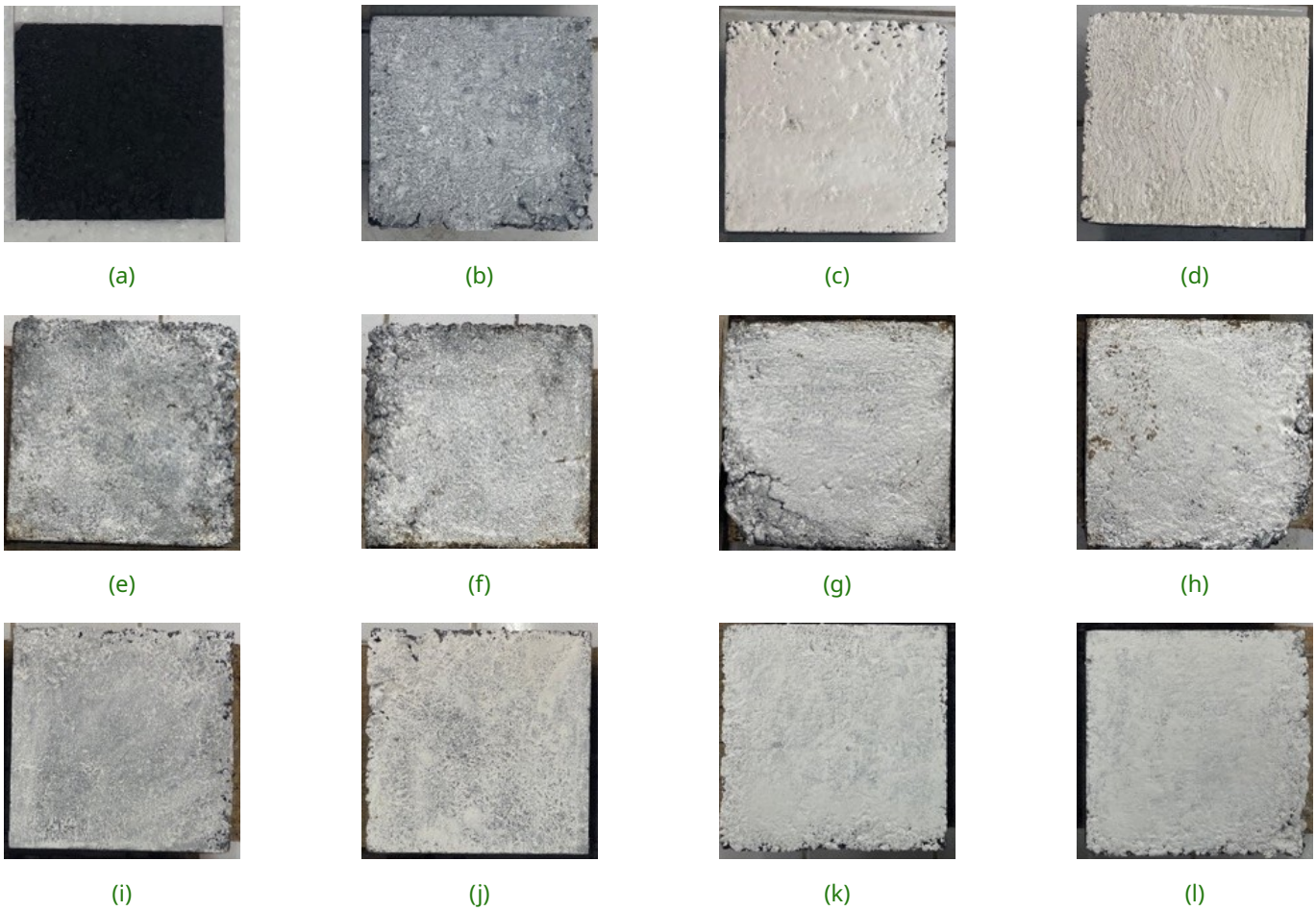

Figure 3 Asphalt slab specimens: (a) uncoated control, (b) white-BC (BeCool formulation), (c) white-EP (epoxy paint), (d) white-AE (acrylic paint), (e–h) hydrated lime (H2) at 50, 100, 150, and 200 g/m^2, and (i–l) hydrated lime (H4) at the same dosages. Each specimen is 30 × 30 cm and prepared in duplicate.

two formulations (H2 and H4) applied at four dosage levels (50–200 g/m^2) (as listed in Table 3 and Table 4). Each variation was prepared in duplicate. Different application techniques were employed depending on the coating material. For HL, application was conducted while the asphalt was still hot, since HL lacks strong adhesion to cooled asphalt surfaces (Zhang et al., 2020). The asphalt surface temperature was carefully maintained at 120 °C, monitored continuously using a non-contact infrared heat gun to ensure uniformity and

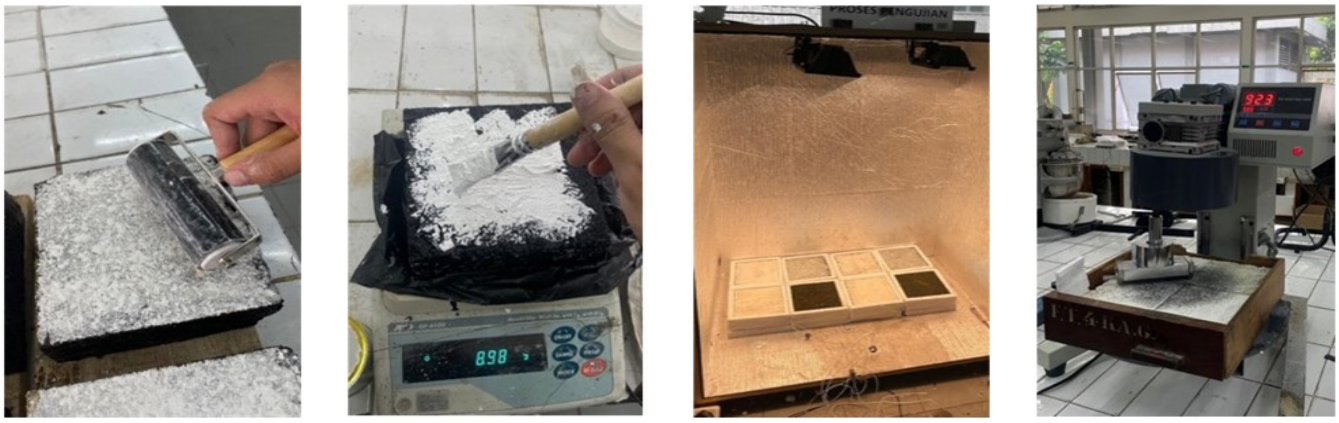

Figure 4 Specimen preparation and testing: (a) compacted HL, (b) spreading HRC, (c) heating–cooling simulation, (d) dry-track abrasion test.

accurate temperature control throughout the process. Once the asphalt reached the target temperature, HL was distributed according to the dosage level and compacted with a rubber roller wrapped in soft tape to enhance surface bonding (Abu-Halimeh, 2007) (Figure 4(a)). Water was lightly applied during rolling to facilitate HL penetration into the surface pores.

In contrast, paint-based coatings were applied on cooled asphalt slabs using a paintbrush at a dosage of 0.6 kg/m² (Yi et al., 2022) (Figure 4(b)). To ensure uniform application and prevent clumping, the coating mixtures were prepared using a high-shear mixer equipped with a variable-speed blade. Each mixture was blended in a 7 cm × 7 cm cylindrical container placed under the mixer blade. For the water-based acrylic formulation, matting agents, dispersants, and defoamers were first mixed for 10 minutes at 150 rpm, followed by the addition of acrylic and TiO_2 for another 10 minutes, and finally, coalescing agents were blended in for 10 more minutes. The epoxy resin variant involved mixing the resin with coalescing agents at 1000 rpm for 10 minutes, then incorporating TiO_2 along with dispersants and defoamers, and continuing the mixing for an additional 15 minutes, followed by a final 10-minute mixing step with coalescing agents. Once the optimal formulation was achieved, coatings were brushed onto asphalt slabs with a uniform thickness of 0.1cm and cured at 25 °C for 24 hours. For the BeCool reflective paint system, the manufacturer's instructions were followed: the primer layer was applied and allowed to dry for 20–30 minutes, followed by the application of the top coating without dilution at 0.25 kg/m².

After curing, each specimen was drilled vertically from the top to a depth of 7.5 cm (measured from the 2.5 cm top surface) to insert a thermocouple (Figure 1(c)). Thermal grease was added to fill the borehole, ensuring efficient heat conduction and eliminating air voids. To restrict heat loss to only the top surface, all lateral sides of the slabs were insulated using polystyrene foam (Alhaqi et al., 2024).

3.2 Methods

3.2.1 Abrasion Test

Abrasion resistance testing was performed to assess the durability of surface coatings applied to asphalt mixtures. The test utilized a wet track abrasion tester (Figure 1(d)), equipped with a loaded wheel applying a total force of 2.5 kg. While this setup does not fully replicate actual traffic loads, it provides a reliable means to evaluate the relative abrasion resistance of the coatings (Han et al., 2020). The test was conducted using a dry method—without water—to simplify the conditions and assess the coatings' initial resistance to wear (Figure 3(c)).

The procedure began with recording the initial weight of each sample. Specimens were then subjected to 2000 abrasion cycles in the testing machine, following the approach described by Momber et al. (2016). After completion, the final weight of each sample was measured. Additionally, the worn surface area was recorded to determine the extent of surface degradation. Performance indicators, including the mass loss (*ML*) and abrasion coefficient (*AC*) were calculated using Equation (1) and Equation (2), as outlined by Rahman et al. (2024).

$$ML = \frac{m_1 - m_0}{m_0} \times 100\% \tag{1}$$

$$AC = \frac{m_1 - m_0}{A_b} \tag{2}$$

where m_0 is the mass of the sample before abrasion; m_1 is the mass after abrasion; A_b is the abraded surface area of the sample.

3.2.2 Heating-Cooling Simulation Test

To replicate the effects of solar heating in a controlled setting, an indoor simulation Figure 1(c) was conducted using a pair of 500 W iodine tungsten lamps, yielding a combined simulated solar irradiance of approximately 1000 W/m², as verified using a pyranometer (Alhaqi et al., 2024). These lamps served as artificial sunlight sources, replicating thermal exposure conditions similar to natural daytime radiation (Pan et al., 2022). The lamps were operated for 12 hours to represent daytime heating and turned off for another 12 hours to simulate nighttime conditions. To ensure uniform thermal conditions and minimize environmental disturbances, the entire setup was housed in a thermally controlled enclosure constructed from wood and lined with reflective aluminum foil, as shown in (Figure 4(c)). The lamps were suspended 75 cm above the asphalt specimens, which were centrally placed within the enclosure. In addition, wind speed and humidity were measured during the test to ensure consistent conditions.

To minimize lateral heat losses, polystyrene insulation was installed around the specimen edges (Figure 4(c)). This setup is consistent with previous experimental protocols reported by Pan et al. (2022) and Chen et al. (2019a). After 24 hours of testing—comprising a full simulated diurnal cycle—temperature data were recorded and evaluated to capture the thermal behavior of each surface treatment configuration.

4 RESULTS AND DISCUSSION

4.1 Initial Thermal Performance

Figure 5 presents the simulated temperature responses of asphalt slabs subjected to 12-hour heating and 12-hour cooling cycles. The results are shown for three surface treatments: (a) paint-based heat-reflective coatings, (b) hydrated lime with No. 200 mesh size, and (c) hydrated lime with No. 400 mesh size. Each subfigure compares coated and uncoated samples over a full 24-hour cycle.

As illustrated in Figure 5, there is a clear temperature distinction between coated (using HRC and HL) and uncoated samples. The horizontal axis represents time in hours, while the vertical axis shows surface temperature in degrees Celsius. During the heating period, all samples exhibited a steady temperature rise, reaching their peak between the 10th and 12th hour. The uncoated sample reached the highest temperature at the end of the heating phase, surpassing 80 °C, reflecting its high heat absorption and low solar reflectivity (Chen et al., 2019b; Wang et al., 2021). In the paint-based HRC group (Figure 5(a)), noticeable surface temperature reductions were observed, with the acrylic-based formulation (White-AE) performing best, followed by the epoxy-based (White-EP) and the commercial Be-Cool (White-BC). This suggests the polymer type and composition significantly influence heat reflectance efficiency.

For hydrated lime surface treatments, both No.200 mesh (Figure 5(b)), and No.400 mesh (Figure 5(c)), groups demonstrated that higher dosages led to better cooling performance. The H2-200 g/m² and H4-200 g/m² samples recorded the lowest peak temperatures in their respective groups, with the latter showing a marginally superior cooling effect. This indicates that finer hydrated lime particles may enhance surface reflectivity due to increased coverage and bonding and Mie scattering (Man et al., 2021). The observed temperature reductions of the coatings suggest the potential to lower pavement temperatures and extend pavement life by slowing material degradation. Broader application could help mitigate urban heat island effects, though long-term field validation under real traffic and environmental conditions is still needed.

Following the heating phase, all samples cooled to approximately 31 °C over a 12-hour period with the halogen lamp switched off, simulating nighttime conditions (cooling phase). During the cooling phase (12–24 hours), all samples showed a gradual temperature decline as external heat sources were removed. Coated specimens—whether with paint-based HRC (Figure 5(a)) or HL treatments (Figure 5(b) and (c))—maintained lower surface temperatures than the uncoated sample throughout this period. This behaviour suggests that these coatings not only reduce heat accumulation during the day but also limit thermal re-radiation at night, which may help mitigate nocturnal ambient temperatures and UHI effects. By the end of each 24-hour cycle, both coated and uncoated surfaces tended to reach similar temperatures, suggesting that the starting temperature on the following day is nearly the same. This is important for UHI mitigation (Han et al., 2023).

For a comprehensive comparison between paint-based HRC and HL treatments, the surface temperature reductions after 12 hours of heating—termed the cooling effect—are presented in Figure 6. These temperature differences reflect the effectiveness of each surface treatment in mitigating heat accumulation. The paint-based group (HRC) exhibited strong performance: the

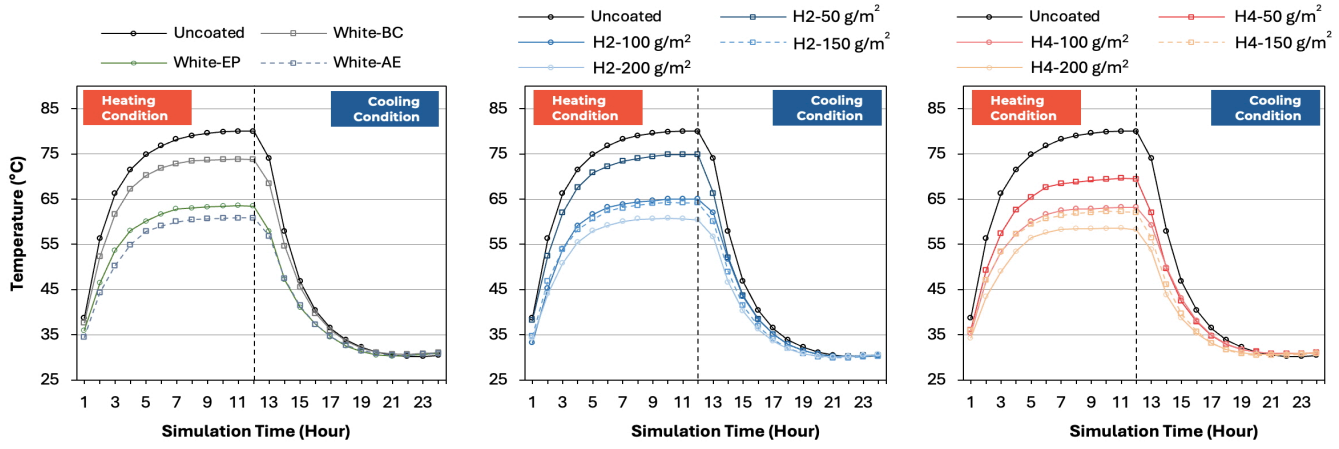

Figure 5 Average temperature of each sample under heating and cooling: (a) paintable HRC, (b) hot-pressed HL (200 mesh), (c) hot-pressed HL (400 mesh).

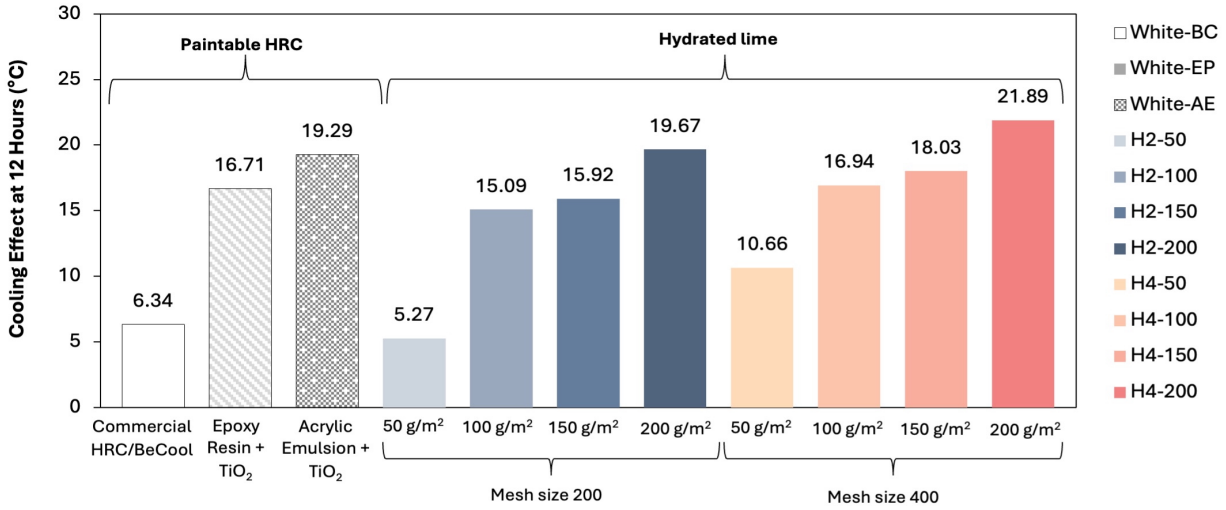

Figure 6 Temperature differences at the end of the heating phase compared to uncoated samples.

acrylic-based coating (White-AE) reduced the surface temperature by 19.29 °C, followed by the epoxy-based (White-EP) and BeCool commercial paint (White-BC). These results confirm the effectiveness of paint-based coatings in minimizing solar heat absorption due to their high reflectivity and film-forming capability.

Meanwhile, the HL-coated samples also performed competitively, with thermal reductions largely influenced by both particle size and dosage. The No.400 HL particles (H4) consistently outperformed the coarser No.200 group (H2), likely due to enhanced coverage and light scattering from finer particles. At the lowest dosage (50 g/m²), H4 achieved a 10.66 °C reduction, while H2 only achieved 5.27 °C. When the dosage increased to 100 g/m² and 150 g/m², H4 showed reductions of 15.92 °C and 18.03 °C respectively, with diminishing returns above 150 g/m². The highest dosage of 200 g/m² resulted in the best performance across both groups: 19.67 °C for H2 and 21.89 °C for H4, which was the greatest reduction among all samples. These findings suggest that, when applied optimally, HL coatings—particularly with finer gradation and higher dosage—can match or even outperform commercial and lab-formulated HRCs in surface temperature mitigation.

A one-way ANOVA test ($p < 0.05$) was used to examine differences in cooling performance among paint-based HRCs (6.34–19.29 °C) and HL coatings (5.27–21.89 °C). The results indicate that higher-dosage HL coatings, particularly H4-200 (21.89 °C) and H2-200 (19.67 °C), provided greater cooling than paint-based HRCs (epoxy and commercial), while acrylic HRC (19.29 °C) showed comparable performance to H2-200. Lower-dosage HL coatings exhibited similar cooling to paint-based coatings, suggesting that application rate strongly influences performance.

4.2 Abrasion Resistance of Surface Coatings

Following the thermal performance evaluation, the coated asphalt samples underwent abrasion testing to assess their resistance to mechanical wear. As shown in Figure 7, the test revealed marked differences in abrasion resistance between the paint-based HRC and the HL treatments. The top graph (Figure 7(a)) illustrates the coating mass loss, while the bottom graph (Figure 7(b)) presents the corresponding abrasion coefficient values.

Quantitatively, mass loss ranged from 0.6 g to 1.3 g across all samples. The highest loss was observed in H2-150 (1.3 g), indicating weaker surface bonding, while H4-100 recorded the lowest (0.6 g), reflecting superior durability. Similarly, higher abrasion coefficient values indicated lower wear resistance. Among paint-based coatings (HRCs), most exhibited moderate to poor abrasion resistance—except for the BeCool (BC) sample, which performed comparatively well with a mass loss of 0.8 g and an abrasion coefficient of 109.64 g/m². In general, HL coatings showed variable wear resistance depending on particle size and dosage. While some HL specimens, particularly those with finer particles (No. 400 mesh) and higher dosages (100–200 g/m²), achieved lower mass losses (0.6–0.8 g) and abrasion coefficients (72–92 g/m²) than paint-based HRCs, others performed similarly or slightly lower. This indicates that HL does not consistently outperform HRCs but can provide superior abrasion resistance when optimized for particle size and application rate.

Two key factors—particle size and dosage—strongly influenced HL coating performance. Regrading dosage, the fluctuations observed at 50 g/m² and 150 g/m² for both mesh sizes are likely influenced by both material behaviour and variability during application. At 50 g/m², limited surface coverage reduces mechanical in-

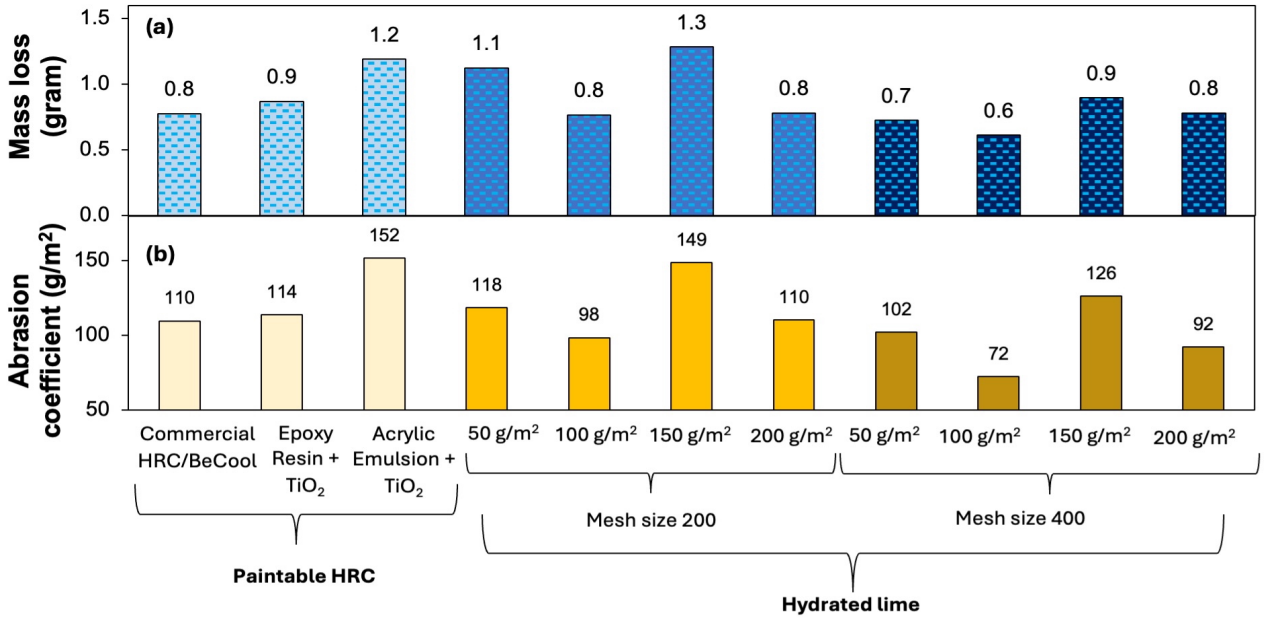

Figure 7 The abrasion resistance test result.

terlock, while 100 g/m² provides more effective bonding and higher resistance. The drop in performance at 150 g/m² is likely due to uneven distribution or agglomeration that weakens bonding efficiency, whereas at 200 g/m², the greater material quantity likely restores surface continuity and improves abrasion resistance. This non-linear trend suggests that abrasion performance depends on dosage, particle packing, and application quality.

In terms of particle size, samples with No.200 mesh particles (H2 group) demonstrated moderate resistance, with mass losses ranging from 0.8–1.3 g and abrasion coefficients of 98.39–148.74 g/m². Meanwhile, the No.400 particle group (H4) outperformed H2, showing mass losses between 0.6–0.9 g and abrasion coefficients of 72.17–126.30 g/m². The superior performance of finer particles is likely attributed to their greater surface area, allowing better penetration into micro-pores and promoting stronger physical and chemical bonding with the asphalt binder (Lebedev et al., 2021). Additionally, higher dosages generally produced better results, with lower application rates (e.g., 50 g/m²) resulting in weaker abrasion resistance.

Visual observations from Figure 8 reinforce these trends. HL-coated specimens with finer particles (e.g., H4-100) retained more material post-abrasion compared to their coarser counterparts (e.g., H2-100), supporting the claim that particle fineness enhances durability. Interestingly, the paint-based coatings presented differing abrasion patterns: although White-AE (acrylic emulsion) recorded higher abrasion losses, it exhibited more uniform surface wear, whereas White-EP (epoxy resin) showed localized and patchy abrasion, which may suggest premature failure in isolated zones under field conditions. This contrast highlights the importance of not only measuring total loss but also considering failure patterns when evaluating long-term surface integrity. In conclusion, both the measurement data and surface observations confirm that HL coatings—particularly those using 400-mesh particles at higher dosages—outperform paint-based alternatives in abrasion resistance.

4.3 Thermal Performance After Abrasion

Following abrasion testing, the coated samples were re-evaluated to determine the effect of surface wear on thermal performance. The analysis focused on the relative temperature change—defined as the difference between pre-abrasion and post-abrasion surface temperatures. This metric indicates the extent of thermal degradation caused by abrasion: a higher value reflects greater loss in cooling performance. As shown in Figure 9, abrasion led to a noticeable decline in thermal performance during both the heating and cooling phases. In the heating phase (Figure 9(a)), temperature differences ranged from 5.8 °C to 8.0 °C, with the smallest change observed in H4-100, indicating its superior retention of thermal reflectivity. In contrast, the greatest performance loss was recorded in H2-50, highlighting its vulnerability to abrasion.

During the cooling phase (Figure 9(b)), the relative temperature changes were smaller, ranging between 1.5 °C and 2.9 °C, suggesting that while abrasion weakened heat dissipation, the effect was less severe than during heat absorption. Overall, the HL coatings—

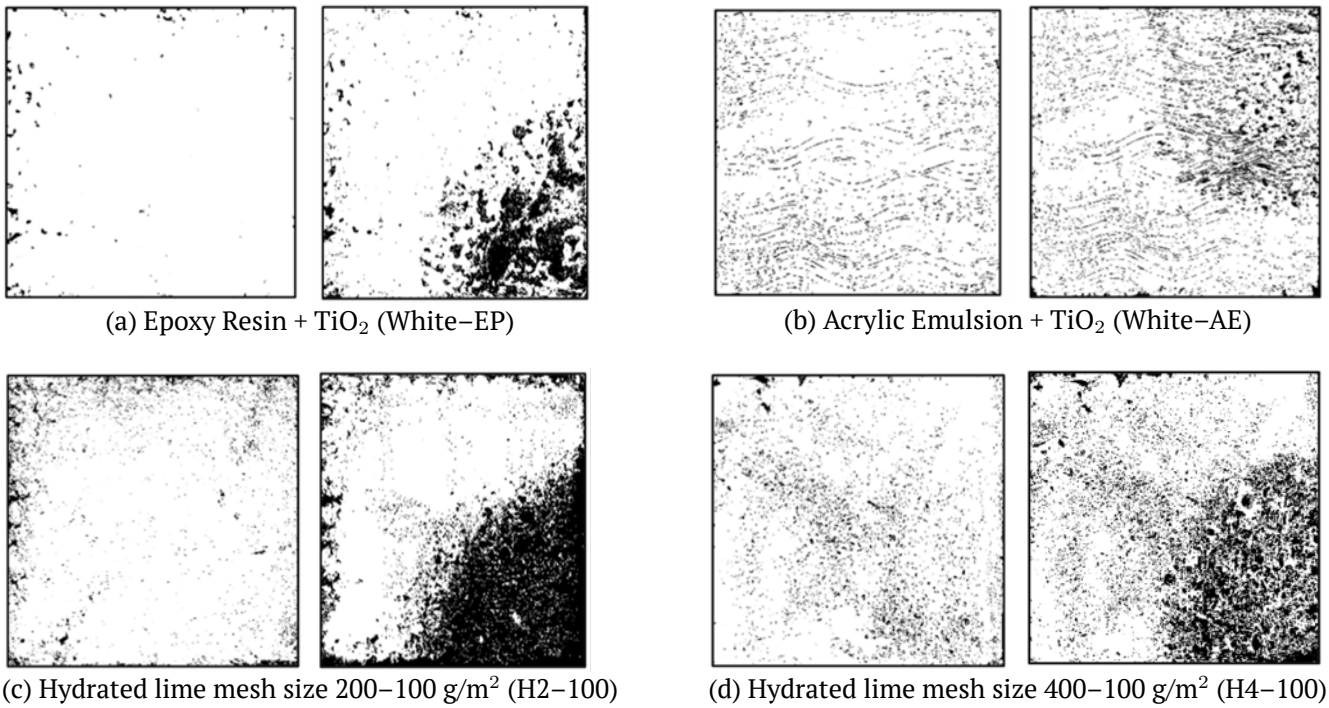

(a) Epoxy Resin + TiO_2 (White–EP)

(b) Acrylic Emulsion + TiO_2 (White–AE)

(c) Hydrated lime mesh size 200–100 g/m^2 (H2–100)

(d) Hydrated lime mesh size 400–100 g/m^2 (H4–100)

Figure 8 Specimens before and after abrasion tests with paint-based HRC and HL at different particle sizes and application rates.

especially those with No.400 mesh particles—exhibited better thermal stability after abrasion compared to paint-based coatings, with H4 variants showing the most consistent performance.

In the paint-based HRC group, BeCool (White-BC) exhibited the greatest increase in surface temperature after abrasion (7.2 °C), indicating the highest thermal degradation. White-AE and White-ER showed similar, moderate increases (6.3 °C). Although White-AE expe-

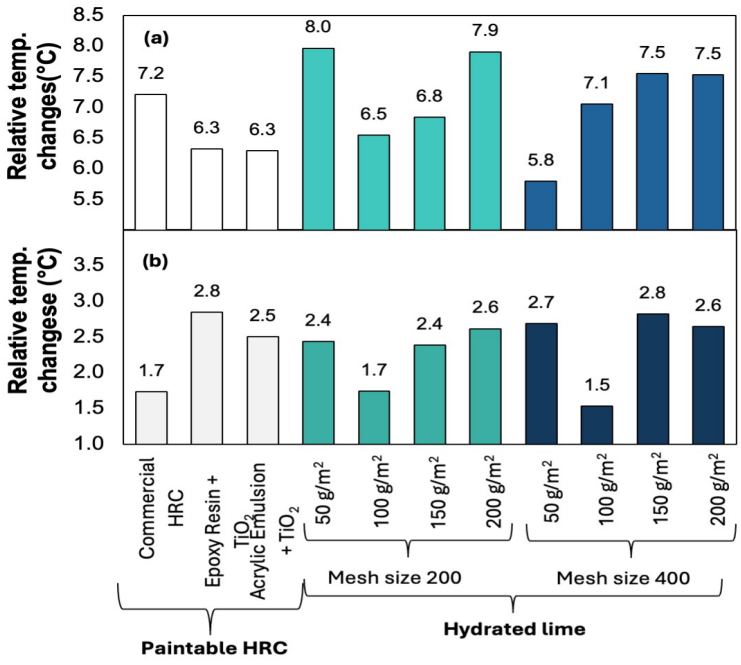

Figure 9 Relative temperature change (ΔT = $T_{initial}$-T_{after}) of coated samples following abrasion: (a) heating phase (12th hour), (b) cooling phase (24th hour). A higher value indicates greater thermal performance degradation due to surface wear.

rienced greater mass loss, it displayed more uniform abrasion, which may help preserve reflectivity better than the patchier wear observed on White-ER.

Abrasion significantly compromises the thermal effectiveness of both coating types. However, hydrated lime (HL) treatments—particularly those using finer particles (No. 400)—demonstrated greater thermal stability after abrasion compared to paint-based HRC Several HL coatings, however, particularly those with larger particle sizes (No. 200) and lower dosages, showed lower performance than HRCs. Notably, for both HRC and HL, all coated samples maintained substantially lower surface temperatures than the uncoated control even after 2000 abrasion cycles, indicating that residual cooling effects remain effective.

Overall, HL presents a promising and cost-effective alternative to conventional HRCs. It offers comparable or superior cooling performance, better abrasion resistance, and more consistent post-wear thermal behaviour. The enhanced abrasion resistance of HL—especially with finer particles—is primarily due to its greater surface area, which allows better penetration into asphalt micro-pores, creating stronger mechanical interlocks. Additionally, HL's inherent hardness and potential for surface hardening through carbonation further improve its durability under mechanical stress. Unlike paint-based HRCs that rely on polymer binders prone to peeling or softening, HL's simpler composition leads to better wear retention and lower degradation under repeated abrasion. Given its affordability and potential lower environmental impact, HL surface treatments appear well-suited as sustainable alternatives for pavement applications. However, long-term studies are needed to assess their durability, skid resistance, and performance under varying environmental conditions.

Lastly, it is important to note that the abrasion tests in this study were conducted under controlled laboratory conditions, which may not fully replicate the complex loading and environmental factors present in actual pavement service. Water immersion effects during abrasion testing were also not examined, even though they could significantly affect coating durability in the field. In addition, the thermal simulation was limited to a 12-hour on/off heating cycle, which does not represent long-term exposure. Future studies should incorporate extended exposure durations, cyclic environmental conditions, and water immersion testing to provide a more comprehensive understanding of coating performance under real-world conditions.

5 SUMMARY AND CONCLUSION

This study investigated the thermal and abrasion performance of paint-based heat-reflective coatings (HRC) and hot-rolled hydrated lime (HL) surface treatments for asphalt pavements, aimed at reducing surface temperatures and mitigating Urban Heat Island (UHI) effects. The main findings are as follows:

1. Both HRC and HL coatings significantly lowered surface temperatures under heating conditions, achieving reductions between 5.27 °C and 21.89 °C. The best performance was recorded by HL with 200 g/m² dosage and 400-mesh particle size (H4-200), while the White-AE (acrylic) HRC also showed strong cooling effect (19.29 °C). The effectiveness of HL is attributed to its enhanced solar reflectivity and diffuse light scattering, particularly in fine-particle formulations that offer better surface coverage and microstructural interaction.
2. In abrasion resistance tests, HL coatings outperformed paint-based HRCs, with mass loss ranging from 0.6 to 1.3 g. Finer HL particles (No.400 mesh) offered greater resistance through higher surface area, micro-pore penetration, and stronger mechanical interlock, while paint-based HRCs generally exhibited weaker surface bonding.
3. After abrasion, all coated surfaces showed temperature increases of 5.8–8.0 °C during heating and 1.5–2.9 °C during cooling. HL coatings—particularly with finer particles—demonstrated better post-abrasion thermal stability than HRCs, indicating more consistent performance after surface wear even though HRCs showed slightly lower absolute increases.
4. Overall, HL surface treatments offer a promising, cost-effective, and environmentally friendly alternative to conventional paint-based HRCs. When optimized in particle size and dosage, HL delivers competitive or superior thermal performance, better abrasion resistance, and more stable residual cooling. Further long-term studies are recommended to assess their durability, skid resistance, and performance under various environmental and traffic conditions.

DISCLAIMER

The authors declare no conflict of interest.

ACKNOWLEDGMENTS

The authors gratefully acknowledge PT Diwangkara Wihaya Nusantara (Driya), the manufacturer of the Be-Cool reflective coating, for providing the commercial materials used in this study.

REFERENCES

Abu-Halimeh, I. (2007), 'Surface colour effects on the thermal behaviour and mechanical properties of hot mix asphalt'.
URL: *http://hdl.handle.net/11375/23207*

Alhaqi, D. H., Nazalanzilni, A. and Rahman, T. (2024), 'Evaluation of the cooling performance of various heat-reflective cool pavement coatings for urban heat island mitigation', *IOP Conference Series: Earth and Environmental Science* **1416**(1), 012005.
URL: *https://doi.org/10.1088/1755-1315/1416/1/012005*

Anting, N., Md. Din, M. F., Iwao, K., Ponraj, M., Jungan, K., Yong, L. Y. and Siang, A. J. L. M. (2017), 'Experimental evaluation of thermal performance of cool pavement material using waste tiles in tropical climate', *Energy and Buildings* **142**, 211–219.
URL: *https://doi.org/10.1016/j.enbuild.2017.03.016*

ASTM (2016), *ASTM D8079-16: Standard Practice for Preparation of Compacted Slab Asphalt Mix Samples Using a Segmented Rolling Compactor*, ASTM International.

ASTM (2020*a*), *ASTM C110-20: Standard Test Methods for Physical Testing of Quicklime, Hydrated Lime, and Limestone*, Annual Book of ASTM Standards.

ASTM (2020*b*), *ASTM E1225–20: Standard Test Method for Thermal Conductivity of Solids Using the Guarded-Comparative-Longitudinal Heat Flow Technique*, Annual Book of ASTM Standards.

Boujelbene, M., Boukholda, I., Guesmi, T., Amara, M. B. and Khalilpoor, N. (2023), 'Solar reflection and effect of roof surfaces material characteristics in heat island mitigation: toward green building and urban sustainability in ha'il, saudi arabia', *International Journal of Low-Carbon Technologies* **18**, 1039–1047.
URL: *https://doi.org/10.1093/ijlct/ctad090*

Cheela, V. R. S., John, M., Biswas, W. and Sarker, P. (2021), 'Combating urban heat island effect—a review of reflective pavements and tree shading strategies', *Buildings* **11**(3), 93.
URL: *https://www.mdpi.com/2075-5309/11/3/93*

Chen, J., Chu, R., Wang, H., Zhang, L., Chen, X. and Du, Y. (2019a), 'Alleviating urban heat island effect using high-conductivity permeable concrete pavement', *Journal of Cleaner Production* **237**, 117722.
URL: *https://doi.org/10.1016/j.jclepro.2019.117722*

Chen, J., Zhou, Z., Wu, J., Hou, S. and Liu, M. (2019b), 'Field and laboratory measurement of albedo and heat transfer for pavement materials', *Construction and Building Materials* **202**, 46–57.
URL: *https://doi.org/10.1016/j.conbuildmat.2019.01.028*

Deilami, K., Kamruzzaman, M. and Liu, Y. (2018), 'Urban heat island effect: A systematic review of spatio-temporal factors, data, methods, and mitigation measures', *International Journal of Applied Earth Observation and Geoinformation* **67**, 30–42.
URL: *https://doi.org/10.1016/j.jag.2017.12.009*

Ega Fajar, W., Entin, H. and Cantika Almas, F. (2025), 'Bioretention design simulation for efficient urban stormwater reduction', *Journal of the Civil Engineering Forum* **11**(1).
URL: *https://doi.org/10.22146/jcef.12806*

Elmagri, H., Kamel, T. M. and Ozer, H. (2024), 'Assessment of the effectiveness of cool pavements on outdoor thermal environment in urban areas', *Building and Environment* **266**, 112095.
URL: *https://doi.org/10.1016/j.buildenv.2024.112095*

Emery, J. J., Guo, P., Stolle, D. F. E., Hernandez, J. and Zhang, L. (2014), 'Light-coloured grey asphalt pavements: from theory to practice', *International Journal of Pavement Engineering* **15**(1), 23–35.
URL: *https://doi.org/10.1080/10298436.2013.782402*

Fathan, A., Noor, M., Maria Grazia, A. and Antonio, C. (2025), 'Advancing road safety in urban area: The impact of roundabouts on intersection design', *Journal of the Civil Engineering Forum* **11**(2).
URL: *https://doi.org/10.22146/jcef.15904*

Güneralp, B., Reba, M., Hales, B. U., Wentz, E. A. and Seto, K. C. (2020), 'Trends in urban land expansion, density, and land transitions from 1970 to 2010: a global synthesis', *Environmental Research Letters* **15**(4), 044015.
URL: *https://doi.org/10.1088/1748-9326/ab6669*

Han, D., Zhang, T., Qin, Y., Tan, Y. and Liu, J. (2023), 'A comparative review on the mitigation strategies of urban heat island (uhi): a pathway for sustainable urban development', *Climate and Development* **15**(5), 379–403.
URL: *https://doi.org/10.1080/17565529.2022.2092051*

Han, S., Yao, T., Han, X., Hongwei, Z. and Yang, X. (2020), 'Performance evaluation of waterborne epoxy resin modified hydrophobic emulsified asphalt micro-surfacing mixture', *Construction and Building Materials* **249**, 118835.
URL: *https://doi.org/10.1016/j.conbuildmat.2020.118835*

Huang, K., Li, X., Liu, X. and Seto, K. C. (2019), 'Projecting global urban land expansion and heat island intensification through 2050', *Environmental Research Letters* **14**(11), 114037.
URL: *https://doi.org/10.1088/1748-9326/ab4b71*

Huang, Z., Gou, Z. and Cheng, B. (2020), 'An investigation of outdoor thermal environments with different ground surfaces in the hot summer-cold winter climate region', *Journal of Building Engineering* **27**, 100994.
URL: *https://doi.org/10.1016/j.jobe.2019.100994*

Ibrahim, S. H., Ibrahim, N. I. A., Wahid, J., Goh, N. A., Koesmeri, D. R. A. and Nawi, M. N. M. (2018), 'The impact of road pavement on urban heat island (uhi) phenomenon', *International Journal of Technology* **9**(8), 1597–1608.
URL: *https://doi.org/10.14716/ijtech.v9i8.2755*

Iizuka, R., Yagi, T., Komatsu, K., Gotou, H., Tsuchiya, T., Kusaba, K. and Kagi, H. (2013), 'Crystal structure of the high-pressure phase of calcium hydroxide, portlandite: In situ powder and single-crystal x-ray diffraction study', *American Mineralogist* **98**(8–9), 1421–1428.
URL: *https://doi.org/10.2138/am.2013.4386*

Kementerian PUPR (2004), Laporan akhir aplikasi pemanfaatan asbuton untuk pemeliharaan jalan, Technical report, Direktorat Prasarana Transportasi.

Lebedev, M., Kozhukhova, M. and Yakovlev, E. (2021), 'The effect of composition and fineness of mineral fillers on structure of asphalt binder', *Materials Science Forum* **1017**, 81–90.
URL: *https://doi.org/10.4028/www.scientific.net/MSF.1017.81*

Li, H. and Xie, N. (2020), Reflective coatings for high albedo pavement, *in* 'Eco-efficient Pavement Construction Materials', Elsevier Inc., pp. 127–146.
URL: *https://doi.org/10.1016/B978-0-12-818981-8.00007-2*

Liu, Y., Li, T. and Peng, H. (2018), 'A new structure of permeable pavement for mitigating urban heat island', *Science of The Total Environment* **634**, 1119–1125.
URL: *https://doi.org/10.1016/j.scitotenv.2018.04.041*

Man, H., Zhang, H. and Jifa, L. (2021), 'Asphalt pavement coated by hot-pressed hydrated lime', *International Journal of Pavement Engineering* **22**(12), 1556–1567.
URL: *https://doi.org/10.1080/10298436.2019.1703980*

Mandal, J., Yang, Y., Yu, N. and Raman, A. P. (2020), 'Paints as a scalable and effective radiative cooling technology for buildings', *Joule* **4**(7), 1350–1356.
URL: *https://doi.org/10.1016/j.joule.2020.04.010*

Mathan, M. and Krishnaveni, M. (2019), 'Monitoring spatio-temporal dynamics of urban and peri-urban land transitions using ensemble of remote sensing spectral indices—a case study of chennai metropolitan area, india', *Environmental Monitoring and Assessment* **192**(1), 15.
URL: *https://doi.org/10.1007/s10661-019-7986-y*

Momber, A. W., Irmer, M., Glück, N. and Plagemann, P. (2016), 'Abrasion testing of organic corrosion protection coating systems with a rotating abrasive rubber wheel', *Wear* **348–349**, 166–180.
URL: *https://doi.org/10.1016/j.wear.2015.11.001*

Mondal, A., Islam, S. S. and Ransinchung, R. N. G. D. (2023), 'Synergistic effect of hydrated lime and warm mix asphalt additive on properties of recycled asphalt mixture subjected to laboratory ageing', *International Journal of Pavement Research and Technology* **16**(4), 968–982.
URL: *https://doi.org/10.1007/s42947-022-00173-y*

Nugroho, R. D., Rahman, T., Utomo, S. H. T. and Suparma, L. B. (2025), 'The effect of surface electric charges in tack coat and aggregate on the interlayer shear-bond strength of asphalt pavements', *Construction and Building Materials* **463**, 140037.
URL: *https://doi.org/10.1016/j.conbuildmat.2025.140037*

Pan, F., Pei, J., Zhang, G., Wen, Y., Zhang, J. and Li, R. (2022), 'Building the cooling roads with high thermal conductivity pavements to relieve urban heat island effect', *Construction and Building Materials* **346**, 128276.
URL: *https://doi.org/10.1016/j.conbuildmat.2022.128276*

Rahman, T., Suhendri, ., Dhaniswara, A., Irawan, M. Z. and Hu, M. (2025a), 'Super cool pavements through passive radiative cooling technology: Modelling and evaluation', *Journal of Road Engineering* .
URL: *https://jre.chd.edu.cn/en/article/id/c59df7bc-7444-46d8-9b34-494d5f944669*

Rahman, T., Suhendri, Tajudin, A. N., Suwarto, F., Sudigdo, P. and Thom, N. (2024), 'Durability evaluation of heat-reflective coatings for road surfaces: A systematic review', *Sustainable Cities and Society* p. 105625.
URL: *https://doi.org/10.1016/j.scs.2024.105625*

Rahman, T., Tajudin, A. N., Wulaningtyas, A. H., Andika, N., Irawan, M. Z. and Widyatmoko, I. (2025b), 'Recent developments in mitigating clogging in permeable pavements: a state-of-the-art review', *Innovative Infrastructure Solutions* **10**(3), 80.
URL: *https://doi.org/10.1007/s41062-025-01882-6*

Rahman, T., Zudhy Irawan, M., Noor Tajudin, A., Rizka Fahmi Amrozi, M. and Widyatmoko, I. (2023), 'Knowledge mapping of cool pavement technologies for urban heat island mitigation: A systematic bibliometric analysis', *Energy and Buildings* **291**, 113133.
URL: *https://doi.org/10.1016/j.enbuild.2023.113133*

Rajagopal, P., Priya, R. S. and Senthil, R. (2023), 'A review of recent developments in the impact of environmental measures on urban heat island', *Sustainable Cities and Society* **88**, 104279.
URL: *https://doi.org/10.1016/j.scs.2022.104279*

Shamsaei, M., Carter, A. and Vaillancourt, M. (2024), 'Utilisation of steel slag aggregates to propose novel asphalt pavement structures alleviating urban heat islands', *Road Materials and Pavement Design* pp. 1–26.
URL: *https://doi.org/10.1080/14680629.2024.2438340*

Vujovic, S., Haddad, B., Karaky, H., Sebaibi, N. and Boutouil, M. (2021), 'Urban heat island: Causes, consequences, and mitigation measures with emphasis on reflective and permeable pavements', *CivilEng* **2**(2), 459–484.
URL: *https://www.mdpi.com/2673-4109/2/2/26*

Wang, C., Wang, Z.-H., Kaloush, K. E. and Shacat, J. (2021), 'Cool pavements for urban heat island mitigation: A synthetic review', *Renewable and Sustainable Energy Reviews* **146**, 111171.
URL: *https://doi.org/10.1016/j.rser.2021.111171*

Wong, T. L. X., Lim, E. L., Mohd Hasan, M. R., Sougui, O. O., Milad, A. and Qu, X. (2024), 'Effectiveness of heat-reflective asphalt pavements in mitigating urban heat islands: A systematic literature review', *Journal of Road Engineering* **4**(4), 399–420.
URL: *https://doi.org/10.1016/j.jreng.2024.04.008*

Xie, N., Li, H., Zhao, W., Zhang, C., Yang, B., Zhang, H. and Zhang, Y. (2019), 'Optical and durability performance of near-infrared reflective coatings for cool pavement: Laboratorial investigation', *Building and Environment* **163**, 106334.
URL: *https://doi.org/10.1016/j.buildenv.2019.106334*

Xie, N., Wang, H. and Feng, D. (2015), Coating materials to increase pavement surface reflectance, *in* F. Pacheco-Torgal, J. A. Labrincha, L. F. Cabeza and C. G. Granqvist, eds, 'Eco-Efficient Materials for Mitigating Building Cooling Needs', Woodhead Publishing, pp. 13–35.
URL: *https://doi.org/10.1016/B978-1-78242-380-5.00002-9*

Yi, Y., Jiang, Y., Fan, J., Zhang, Y., Deng, C., Tian, T. and Ji, X. (2022), 'Durability of a heat-reflective coating on an asphalt pavement', *Road Materials and Pavement Design* **23**(11), 2651–2668.
URL: *https://doi.org/10.1080/14680629.2021.1991838*

Zhang, H., Quan, W., Liu, J. and Lai, F. (2020), 'Thermosetting powder coating for asphalt pavement', *Road Materials and Pavement Design* **21**(1), 217–236.
URL: *https://doi.org/10.1080/14680629.2018.1484383*

Zheng, N., Lei, J., Wang, S., Li, Z. and Chen, X. (2020), 'Influence of heat reflective coating on the cooling and pavement performance of large void asphalt pavement', *Coatings* **10**(11), 1065.
URL: *https://www.mdpi.com/2079-6412/10/11/1065*